



Growth and transparent substrates effect on Sn₂S₃ thin films obtained via physical solid interactions

A. Timoumi^{1,*} , R. Alzahrani¹, and G. Alsherif¹

¹Department of Physics, Faculty of Applied Science, Umm AL-Qura University, Makkah 21955, KSA, Saudi Arabia

Received: 12 January 2023

Accepted: 23 April 2023

Published online:
12 May 2023

© The Author(s), under exclusive licence to Springer Science+Business Media, LLC, part of Springer Nature 2023

ABSTRACT

In this study, a novel formulation for the production of Sn₂S₃ powder from solid reaction is proposed, with tin and sulfur source serving as the key precursor compounds. Single thermal evaporation source was used to produce Sn₂S₃ thin films. The samples were identified and measured using XRD, XPS, OM, SEM, AFM, Raman spectroscopy, and UV–vis spectroscopy. Sn₂S₃ film characteristics are influenced by the transparent substrates that are used. The choice of substrate affects the sample surface’s homogeneity and RMS roughness. The optical band gap energy was determined in the range of (2.22–2.75) eV range for direct transition. The outcomes of this research are applicable to photovoltaic and optoelectronic devices.

1 Introduction

Tin sulfide is a well-known semiconductor that is frequently manufactured in the modern fields of physics-chemistry, nanotechnology, and nanomaterials [1]. Due to their superior ionic intercalation abilities, sulfur ions integrate both metallic and non-metallic components into complex structures [2, 3]. Compared to their cadmium and indium counterparts used in solar cells [4–8] and optoelectronics [9, 10], Sn and S are more common in nature, less expensive, and less poisonous [4, 5]. In the production of hybrid thin films of SnS₄ and CuInSe₂ the compounds can be replaced by Cu₂ZnSnS₄ to obtain a material with solar conversion parameters like those established [8, 11]. The SnS₂ hexagonal and orthorhombic Sn₂S₃ deposited in thin films as semiconductor and window material are the most

prevalent SnS₂ crystal forms, and the Sn_xS_y compounds crystallize in various phases with at least three basic forms that are categorized according to their stacking sequence [12–14]. Thin films of SnS, a cadmium-free buffer, were first produced in Sn/S/O layers by evaporation for solar cells, resulting in a bandgap of 1.1 to 1.5 eV, strong optical absorption, and intrinsic conductivity type p [15]. Heterojunctions based on SnS and SnS₂ compounds have been produced in 2015 using plasma enhanced chemical vapor deposition (PECVD) [16]. SnCl₂ and N,N-dimethyl thiourea were used as precursors to develop thin films of SnS₂ in 2007 utilizing the pyrolytic spray approach, with alcohol, water, and hydrochloric acid serving as solvents [1, 11, 17]. Following that, a method for producing tin sulfide nanoparticles by directly dispersing molten tin in solution with sulfur was reported [3, 13]. That same

Address correspondence to E-mail: aotemoume@uqu.edu.sa

year, microelectronic applications of monocrystalline SnS nanowires produced and deposited by thermal evaporation under hydrogen argon atmosphere using a quartz tube furnace on gold-coated silicon substrates were also reported [9]. Recently, orthorhombic phase SnS thin films were formed utilizing the SILAR method from tin chloride and ammonium sulfide, with a crystal size of 45 nm and a bandgap of 1.63 eV [18]. Then, in 2016 [19], thermal evaporation was used to form thin films of nanospheres in the orthorhombic phase for SnS and Sn₂S₃ and the hexagonal phase for SnS₂. As a result, we made the decision to focus our study on tin sulfide thin films. Because of their optical properties, they are used in thin-film solar cells as absorbers and window layers. As well as electrical qualities, Sn₂S₃ crystallizes in a rhombic crystal form with a bandgap ranging from 0.95 eV [20] to 2.2 eV [21] Sn₂S₃'s excellent isotropic conductivity makes it a good semiconducting material for constructing p-n or p-i-n solar systems. We obtained new physical synthesis under pressure at 25 °C, using inexpensive chemicals, and with simple residual control. The process is based on adding metallic tin and sulfur powder in the single source.

In this work and based on our previous work [22–30], we provide examples of how various thermal processing methods enhance the crystalline quality and characteristics of physically formed Sn₂S₃ thin films. Particularly, we reported a new approach to synthesis of Sn₂S₃ thin film of 70 nm deposited on different substrates. We expect that this research will provide novel design ideas for tin sulphide solar cell structures.

2 Experimental

2.1 Synthesis

Thin sheets of Sn₂S₃ were deposited on glass, SnO₂, ITO, and FTO. The glass sample was first washed with water and a disinfectant before being dried, submerged in distilled water for a short period of time, and then submerged in a 50 ml nitric-acetic solution for ten minutes. Substrates were finally dried and put into ethanol. A crucible made of graphite is heated with 0.2 g of powdered Sn₂S₃ material.

Figure 1 depicts the schematic layout of a single thermal evaporator in use. The substrate is positioned in the crucible at a height of 10 cm and in a high vacuum atmosphere with a pressure of up to 10⁻⁶ torr. By applying a high current voltage between 40 and 50 amperes, the source is heated. The source is heated until the materials inside are liquid at their melting points (231.9 °C for tin and 112.8 °C for sulfur). The steam will flow above the source and come into touch with the substrate when these materials vaporize. Twenty minutes later, Sn₂S₃ thin films are created and the surface that was previously deposited is coated.

2.2 Techniques for characterization

X-ray diffraction (XRD) patterns were used to examine the structural characteristics. Using the Ultima IV model and Cu-K radiation (1.541874 Å), thin films were produced. Spectroscopy using Raman It was carried out utilizing 785 nm Raman spectroscopy at room temperature. Optical microscopy, scanning electron microscopy (SEM), and atomic force microscopy were used to study morphological aspects (AFM). Thin films' optical transmittance (T) and absorbance (A) spectra were measured in the 190–2500 nm wavelength range.

3 Results and discussion

3.1 Structural characteristics

According to XRD measurements used to look for any changes in the crystal spectrum, Sn₂S₃ films have been investigated. The Sn₂S₃/glass sample is amorphous, as seen in Fig. 2. The heightened material-substrate contact brought on by the precipitates' haphazard stacking is what is responsible for the poor film crystallization and low intensity. The study showed that the films deposited exhibit sharp peaks in their XRD patterns, with the best peaks occurring at (141), (250), (241) and (080) which equate to 26°, 27°, 48° and 52°, respectively. These values closely match those on the Sn₂S₃ standard card (JCPDS 14–0169) [31]. Using Scherrer's formula [32] from the literature, the crystal size of Sn₂S₃ thin films deposited on various substrates was evaluated from the XRD patterns using the Scherrer Eq. (1):

Fig. 1 Schematic for a single source of thermal evaporation utilized in synthesis process

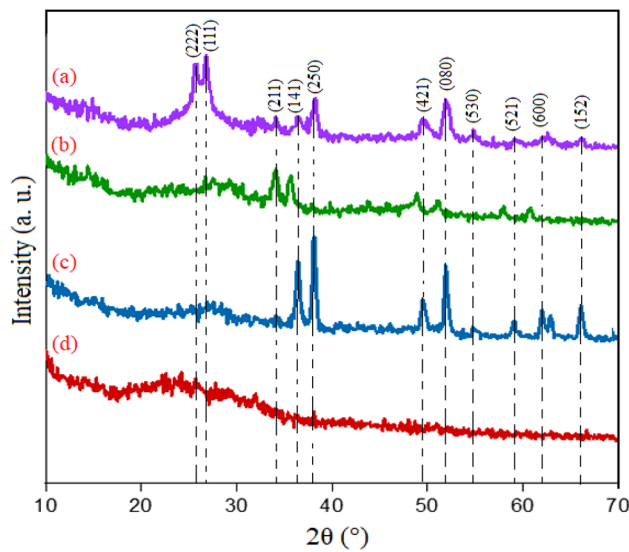
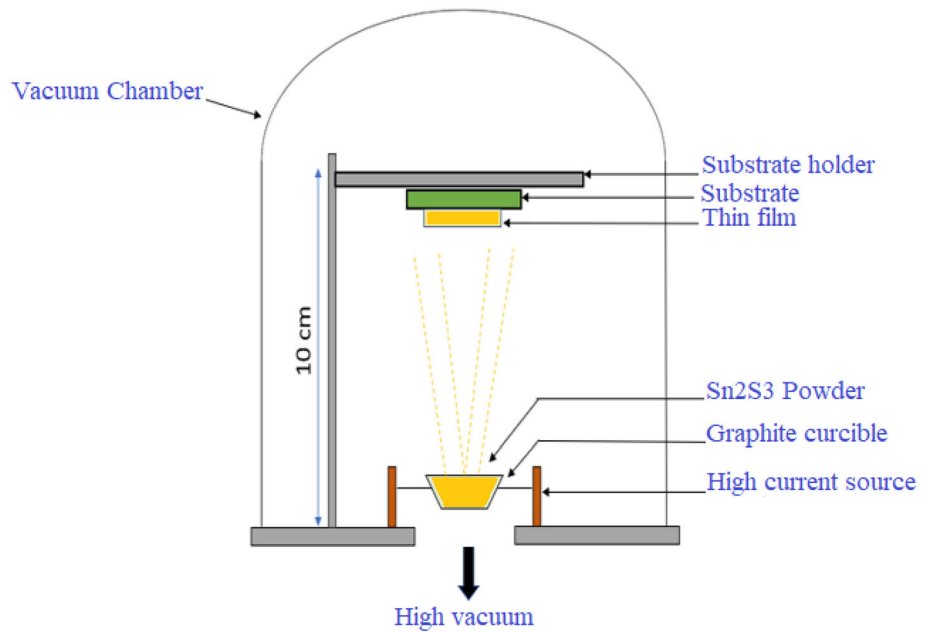


Fig. 2 Patterns of Sn₂S₃ thin films grown at **a** SnO₂, **b** ITO, **c** FTO and **d** glass substrates as shown by X-ray diffraction

$$D = \frac{0.9\lambda}{\beta \cos \theta}, \tag{1}$$

where θ is the Bragg angle, λ is the X-ray radiation’s wavelength (1.54 Å), and β is the peak’s full width at half maximum (FWHM). Table 1 lists the FWHM and average crystallite size values for as-deposited Sn₂S₃ thin films. It is reported that the instrumental broadening and physical elements such crystallite size, micro strain, and dislocation density affect the

XRD peak width of thin films. Utilizing the following formula (Eq. 2), the micro strain (ϵ) is determined:

$$\epsilon = \frac{\beta \cos \theta}{4 \sin \theta} \tag{2}$$

The dislocation density is deduced and calculated using the formula (Eq. 3) where (D) is the crystallite size deduced from (Eq. 1):

$$\delta = \frac{1}{D^2} \tag{3}$$

3.2 Raman analysis

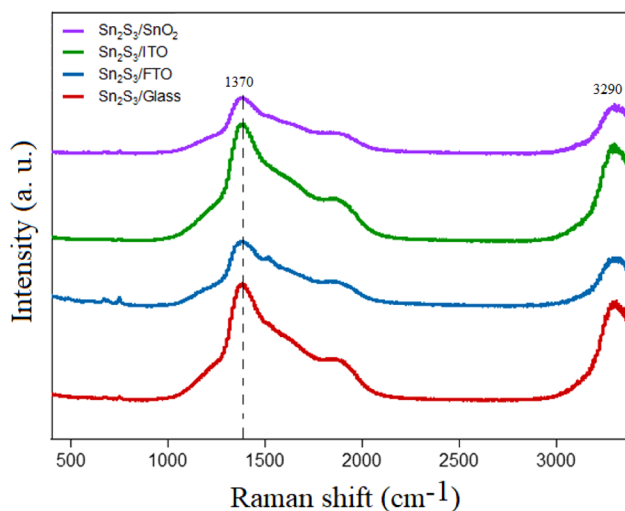
Figure 3 displays the 400–3500 cm⁻¹ range of Sn₂S₃ thin film Raman spectra. This verifies the XRD findings because we can see that all of the peaks had the same pattern on various substrates. Raman investigations at 1370 and 3290 cm⁻¹ reveal various particular ranges. Furthermore, no notable peak shift or broadening is seen in the Raman spectra, proving that the films are strain-free. The Sn₂S₃ phase is practically located at (304 cm⁻¹) [33].

3.3 XPS analysis

The glass slide was employed as the primary substrate for the XPS measurements, from which certain signals of elements like silicon and amplified oxygen were received. Figure 4 displays a survey spectrum where Sn, S, O, and C, among other elements, can be

Table 1 Sn₂S₃ layer structural characteristics

| Substrate Type | 2 θ (°) | FWHM (β) radians $\times 10^{-3}$ | Crystallite size (nm) | Micro stain (ϵ) $\times 10^{-3}$ | dislocation density (δ) (m ⁻²) $\times 10^{-5}$ |
|------------------|----------------|--|-----------------------|---|--|
| Glass | — | — | — | — | — |
| FTO | 38.1 | 7.3 | 194 | 8.9 | 2.65 |
| ITO | 38.1 | 2.1 | 67 | 2.6 | 22.3 |
| SnO ₂ | 38.1 | 4.1 | 35 | 5.0 | 81.6 |

**Fig. 3** Sn₂S₃ thin film Raman spectra on various substrates

seen. For Sn₂S₃ thin films, XPS broadband scanning was recorded from 0 to 1000 eV, allowing us to count the inclusions and identify the components on the sample surface. Figure 4 displays the X-ray photoelectron spectroscopy (XPS) measurements, which shows that no contaminants were found. As a result of surface contamination, XPS peaks are seen at 284 and 530 eV that are attributed to C1s and O1s, respectively [34, 35].

3.4 Optical microscopy properties

After conducting any experiment in the lab, we are supposed to resort to taking magnified optical microscopy (OM) images that appear at the micrometer level, as shown in Fig. 5a Sn₂S₃/glass, where some impurities appeared that may be due to the solvents suspended in it after the cleaning process. As shown in Fig. 5b–d, cap molecules are evenly distributed in the form of spots on the surface and the films show a high-quality image. The shape of the film changes depending on the type of substrate. The

grain development and microcrystalline structure of the precipitate is affected differently by different substrates. These changes have a direct impact on the film's optoelectronic specifications and performance. For all these reasons, the substrate, and the material to be coated must be they are chemically compatible and do not react (Fig. 6).

3.5 SEM analysis

Figure 7 shows the surface and the cross-sectional SEM images of obtained samples deposited on various substrates. Figure 6a shows that Sn₂S₃ deposited on glass is seen as large randomly scattered grain-shaped crystals with gaps. In Fig. 6b, thin films of Sn₂S₃ deposited on FTO are very smooth, compact, and tightly packed. Randomly oriented holes can be observed in the grown film. Larger grains with less hole are scattered homogeneously in the FTO sample, with increase of particle size of Sn₂S₃ thin film deposited on ITO and SnO₂ in Fig. 6c, d. These images revealed that the surface of SnO₂ was denser, with fewer voids and vacancies, when compared to ITO sample, which contains tiny particles. In addition, cross-sectional SEM images (Fig. 6a'–d') for all samples are made to observe their adhesion of Sn₂S₃ on different samples.

3.6 The AFM analysis

Surface morphological changes were monitored using AFM, which was also utilized to assess surface roughness and film morphology. Figure 7 displays two-dimensional (2-D) and three-dimensional (3-D) atomic force microscopy images of thin Sn₂S₃ films that were captured with a 1.4 cm \times 1.4 cm scanning area. Both the films formed on glass and ITO have a distinct and consistent shape. A hill-like surface with pointed peaks makes up the surface of the films.

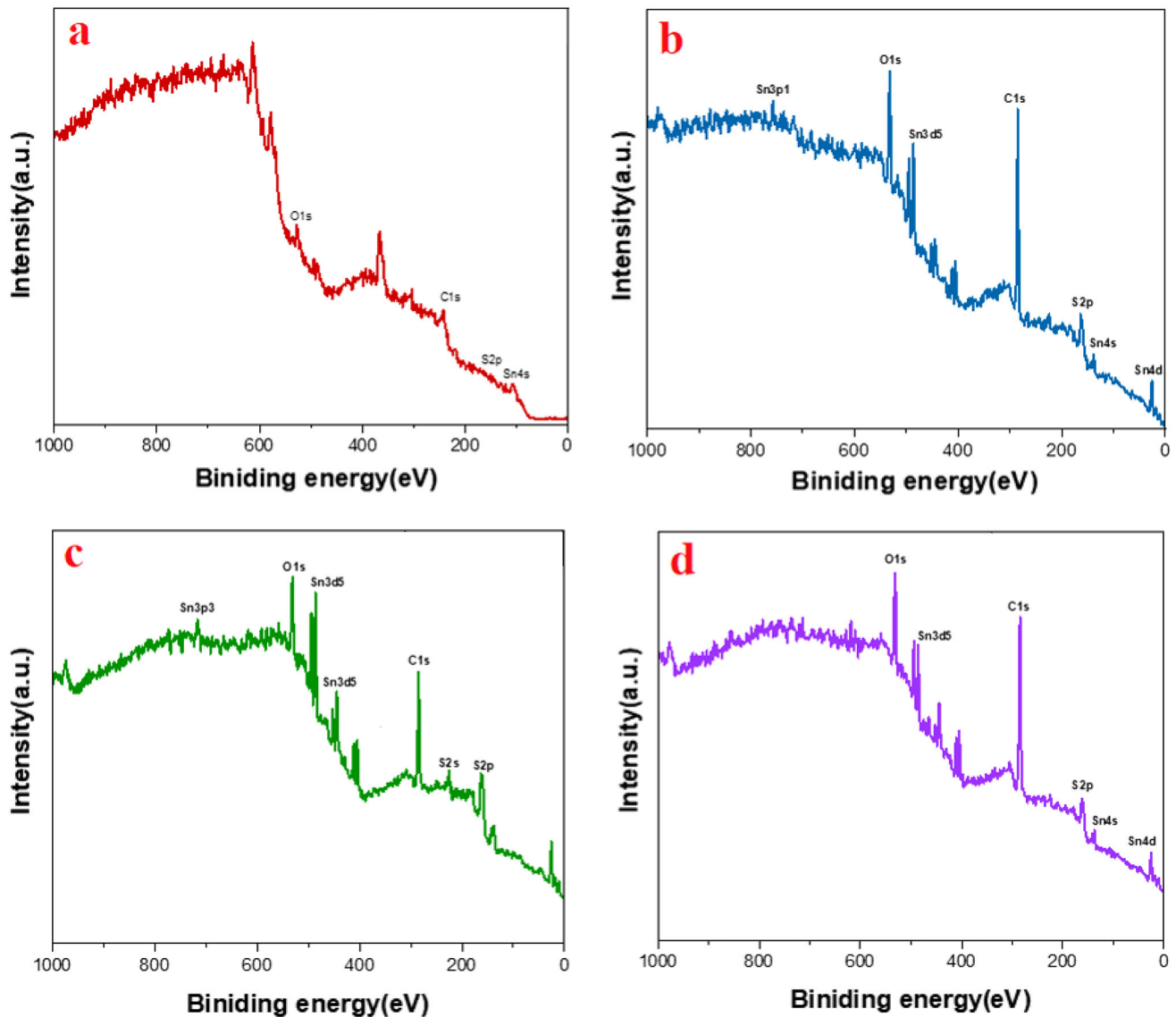


Fig. 4 XPS survey spectrum of Sn_2S_3 thin films released on several substrates, including **a** glass, **b** FTO, **c** ITO, and **d** SnO_2

AFM is used to estimate the films' grain size and surface roughness (rms). Table 2 displays the samples' surface roughness (rms) values. A smooth surface with evenly spaced grains and one emerging vertex was discovered for the Sn_2S_3 /glass sample. Images are unable to show the secondary phase's formation at the grain boundaries as islands.

3.7 Optical characteristics

At room temperature, a UV–visible spectrophotometer was used to examine the optical properties of Sn_2S_3 thin films in the 190–2500 nm wavelength

range. Figure 8 displays the absorbance vs. wavelength graph. The absorbance of the films decreases slightly as wavelength increases. The findings show that the thin films of precipitated Sn_2S_3 have low UV, VIS, and NIR absorption values. This slight change in absorbance has an impact on other optical properties as well. Low absorption values between 500 and 1244 nm were found in the results. At 267 nm, the absorption value was at its greatest (4.6). Figure 9 displays the transmittance vs. wavelength graph. With increasing wavelength, precipitated coatings transmit light more effectively. According to the findings, Sn_2S_3 thin films exhibit a high percentage of

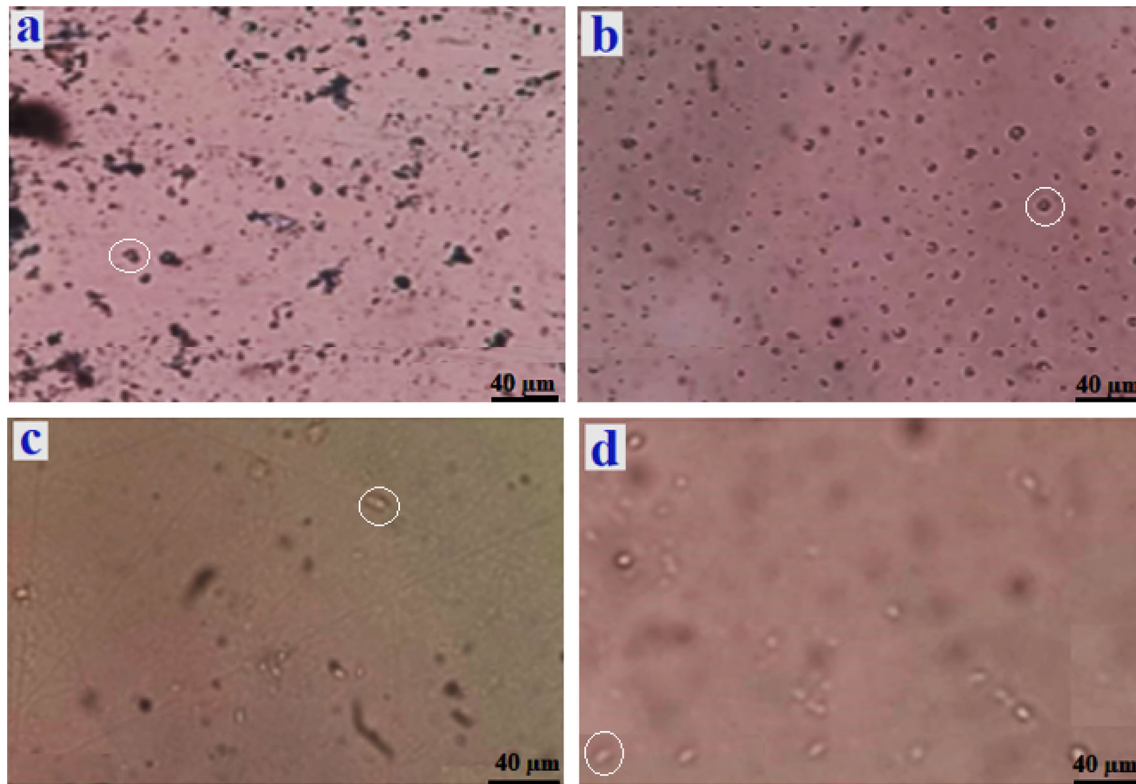


Fig. 5 Optical microscope photographs of Sn_2S_3 thin films that were grown on several substrates, including **a** glass, **b** FTO, **c** ITO, and **d** SnO_2

transmittance in the UV, VIS, and NIR wavelength ranges. The greatest transmittance value for glass and SnO_2 samples is 90.7% at 2234 nm.

The following relationship can be used to calculate the absorption coefficient α [35]:

$$\alpha = \frac{1}{d} \times \ln \frac{(1 - R)^2}{T}, \quad (4)$$

where d represents the thin film's thickness. Using a surface determination equipment, the sample's thickness was determined to be 70 nm.

The Tauc formula is used to calculate the optical bandgap energy [35]:

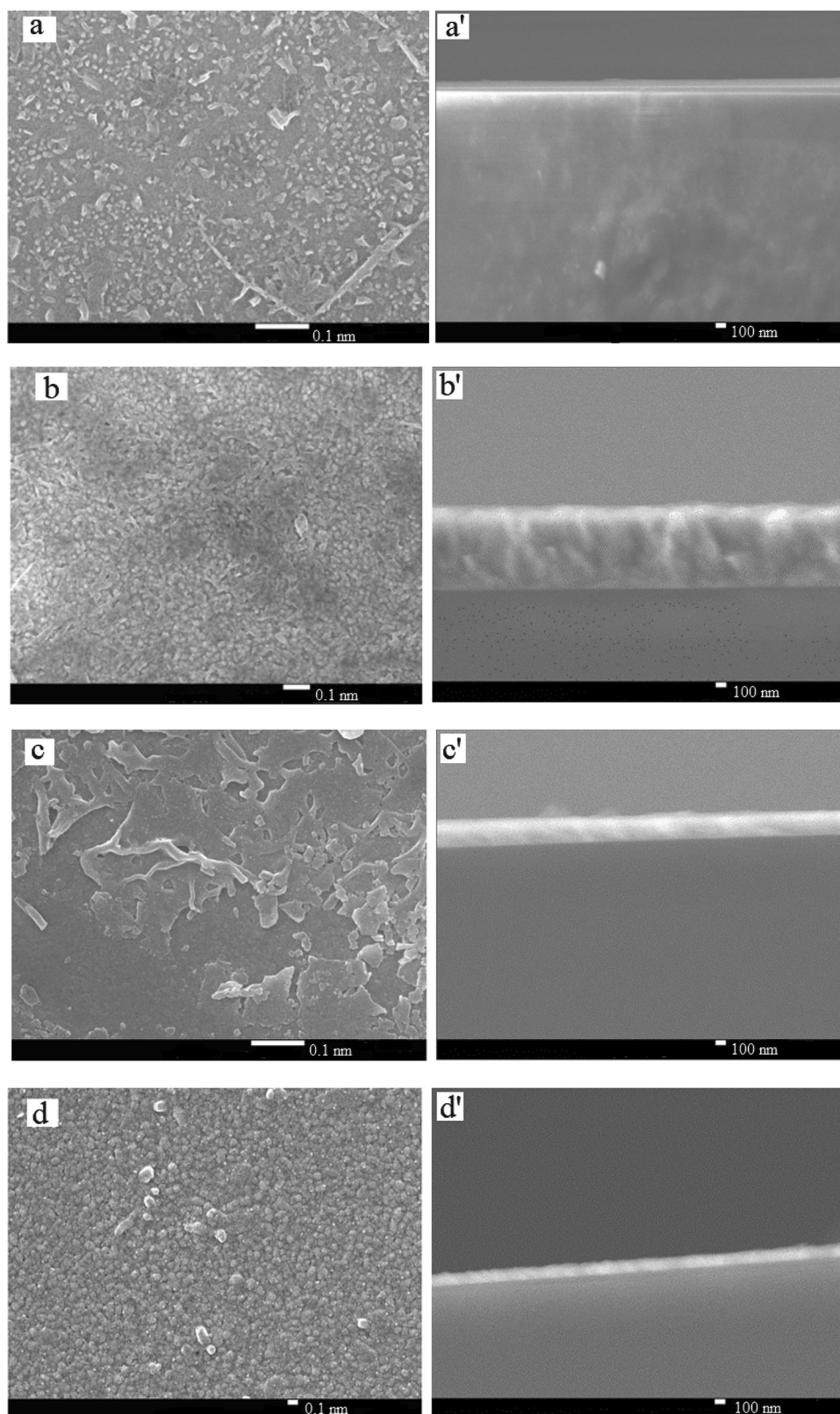
$$(\alpha h\nu)^{\frac{1}{r}} = A(h\nu - E_g), \quad (5)$$

where A is the constant that does not depend on photon energy, the Planck constant is h , $(h\nu)$ is the incident photon energy, E_g is the bandgap energy and $1/r = 2$ for the direct transition's probability. Figure 10 demonstrates that the bandgap values of the measured materials ranged between 2.22 and 2.75 eV and converged to the value reported in the literature [36].

4 Conclusion

Single thermal evaporation process was used to deposit Sn_2S_3 thin films on various substrates. We were able to show through the results that the quality of the substrate being used had an impact on the films' quality. While the quality of the films was on the surfaces of other substrates, microscopic analysis revealed the presence of contaminants on the surface of the glass sample. SEM research shows that the microstructure was in charge of determining how the films' surfaces were shaped. AFM detected an increase in surface roughness (rms) of 21 nm and 40 nm. Raman spectroscopy exhibits two distinct peaks for Sn_2S_3 at 1386.7 cm^{-1} and 3306.5 cm^{-1} . All films were found to have direct optical band gaps between 2.22 and 2.75 eV, which makes them ideal for photovoltaic applications, according to an optical research. The developed recipe is reproducible, it suggests that under typical lab conditions, the films produced are very stable.

Fig. 6 SEM images and cross-sections of Sn_2S_3 thin films formed on several substrates including **a-a'** glass, **b-b'** FTO, **c-c'** ITO, and **d-d'** SnO_2



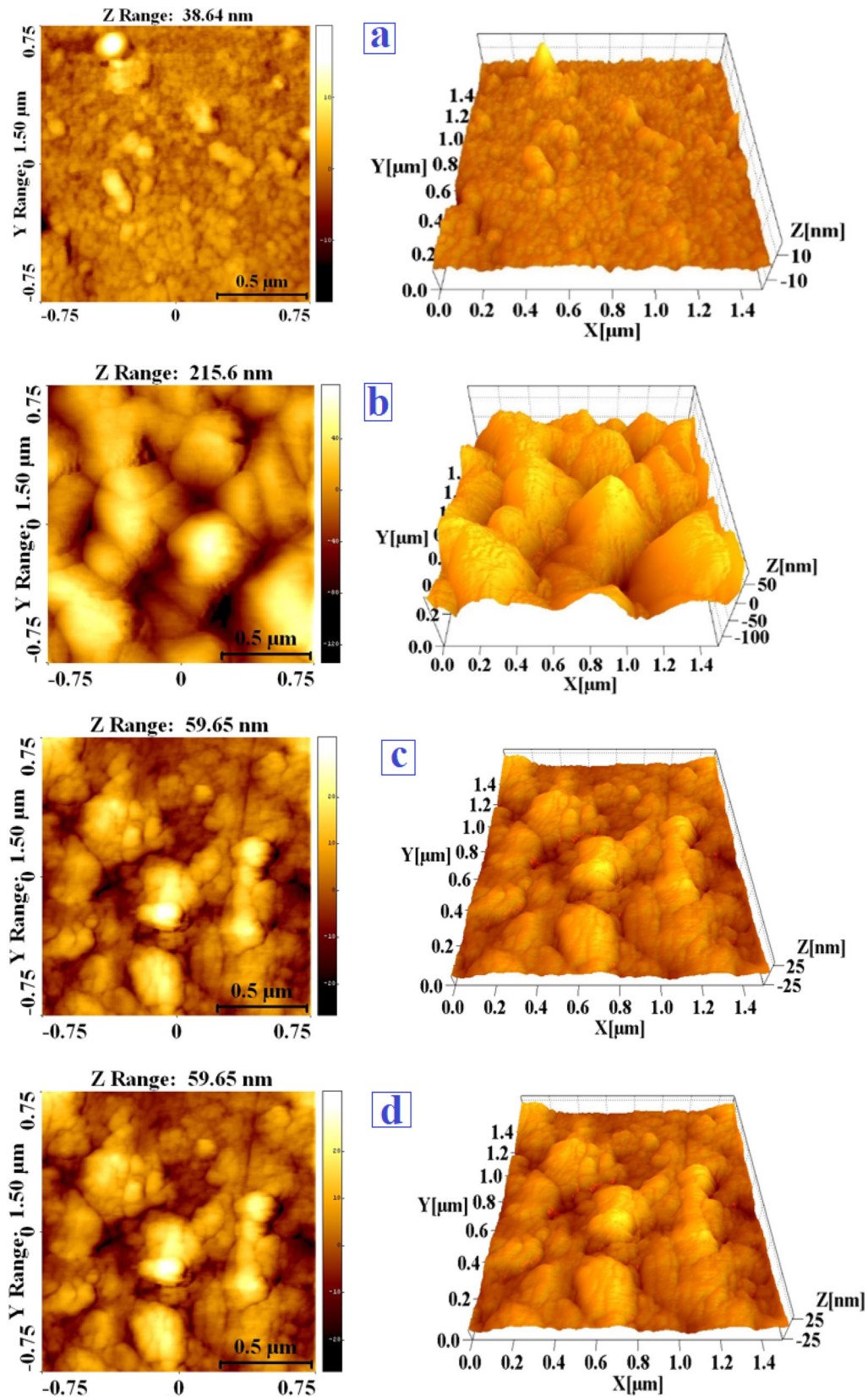


Fig. 7 2D and 3D AFM analysis Sn_2S_3 thin films formed on several substrates including **a** glass, **b** FTO, **c** ITO, and **d** SnO_2

Table 2 Roughness of the Sn₂S₃ thin films' surfaces on various substrates

| Substrate Type | The surface roughness (rms) |
|------------------|-----------------------------|
| Glass | 21 nm |
| FTO | 35 nm |
| ITO | 40 nm |
| SnO ₂ | 27 nm |

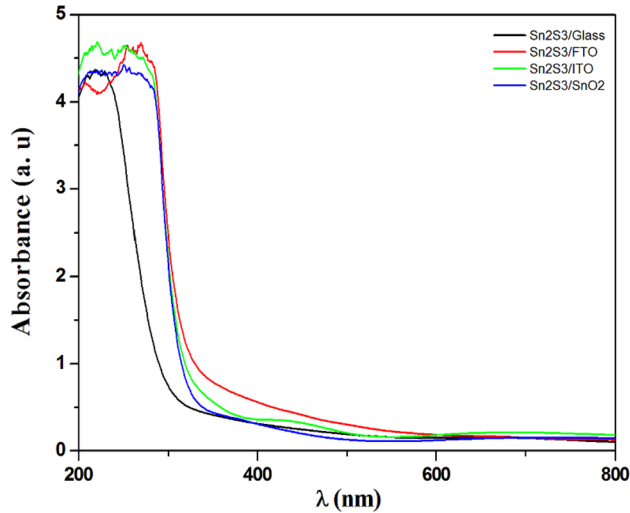


Fig. 8 Spectra of absorption for the Sn₂S₃ thin film layers

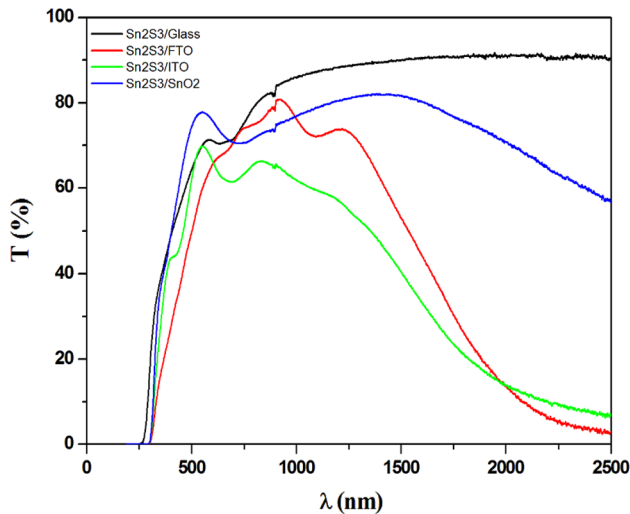


Fig. 9 Sn₂S₃ thin film optical transmission of the obtained layers

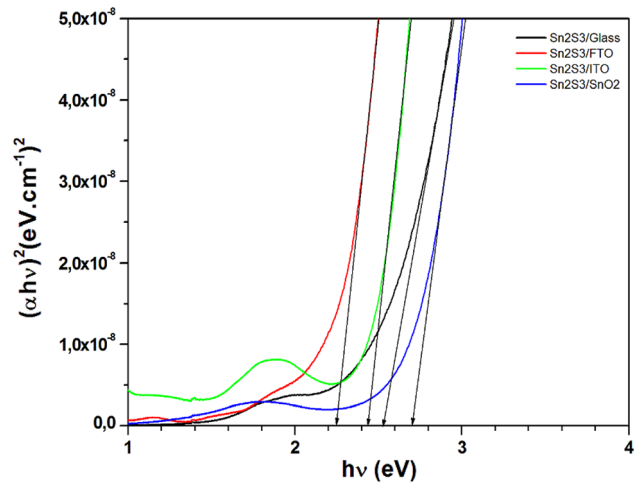


Fig. 10 The plot $(\alpha hv)^2$ vs. (hv) for the Sn₂S₃ thin layers

Acknowledgements

The authors would like to acknowledge Deanship of Scientific Research at Umm Al-Qura University, Makkah for supporting this work by Grant Code: (23UQU4331172DSR002).

Author contributions

The authors have to mention the role of each author in the paper. The roles are below. This is available in the submission instructions. AT: Investigation, Supervision, Data curation, Methodology, draft preparation, Writing– review & editing. RA: Investigation, Data curation, Writing. GA: Investigation, Data curation.

Data availability

The data that support the findings of this study are available from the corresponding author upon reasonable request.

Declarations

Conflict of interest On behalf of all authors, the corresponding author states that there is no conflict of interest.

Research data Policy These policies make it easier for researchers to share data and files that support their publications and improve author service and experience.

References

1. T. Jiang, G.A. Ozin, *J. Mater. Chem.* **8**(5), 1099 (1998)
2. J. Gaur, S. Jain, S. Chand, N.K. Kaushik, *Am. J. Anal. Chem.* **5**, 50 (2014)
3. K. Li, S. Yan, Z. Lin, Y. Shi, *J. Alloy. Compd.* **681**, 486 (2016)
4. H. Katagiri, K. Jimbo, W.S. Maw, K. Oishi, M. Yamazaki, H. Araki, A. Takeuchi, *Thin Solid Films* **517**, 2455 (2009)
5. K. Muska, M. Kauk, M. Altosaar, M. Pilvet, M. Grossberg, O. Volobujeva, *Energy Procedia* **10**, 203 (2011)
6. C. Calderón, G. Gordillo, E. Banguero, P. Bartolo-Pérez, M. Botero, *Revista Mexicana de Física* **62**, 484 (2016)
7. T.J. Whittles, L.A. Burton, J.M. Skelton, A. Walsh, T.D. Veal, V.R. Dhanak, *Chem. Mater.* **28**, 3718 (2016)
8. F. Hergert, R. Hock, *Thin Solid Films* **515**, 5953 (2007)
9. S.R. Suryawanshi, S.S. Warule, S.S. Patil, K.R. Patil, M.A. More, *ACS Appl. Mater. Interfaces* **6**, 2018 (2014)
10. A. Sanchez-Juarez, A. Ortiz, *J. Electrochem. Soc.* **147**(10), 3708 (2000)
11. K. Jimbo, R. Kimura, T. Kamimura, S. Yamada, W.S. Maw, H. Araki, K. Oishi, H. Katagiri, *Thin Solid Films* **515**, 5997 (2007)
12. V. Robles, J.F. Trigo, C. Guillén, J. Herrero, *Energy Procedia* **44**, 96 (2014)
13. Y. Zhao, Z. Zhang, H. Dang, W. Liu, *Mater. Sci. Eng., B* **113**, 175 (2004)
14. O.E. Ogah, G. Zoppi, I. Forbes, R.W. Miles, “23rd European Photovoltaic Solar Energy Conference”, Valencia Spain, 1–5 (2008).
15. L.S. Price, I.P. Parkin, A.M.E. Hardy, R.J.H. Clark, *Chem. Mater.* **11**, 1792 (1999)
16. A. Sanchez-Juarez, A.T. Silver, A. Ortiz, *Thin Solid Films* **480–481**, 452 (2005)
17. M.C. Rodríguez, A.S. Juárez, *Superficies y Vacío* **20**(1), 34–38 (2007)
18. A. Mukherjee, P. Mitra, *Mater. Sci.-Pol.* **33**(4), 847 (2015)
19. F. Sheini, M. Cheraghizade, R. Yousefi, *Sol. Energy Mater. Sol. Cells* **154**, 49 (2016)
20. U.V. Alpen, J. Fenner, E. Gmelin, *Mater. Res. Bull.* **10**(3), 175–180 (1975)
21. M. Khadraoui et al., *Solid State Commun.* **150**(5–6), 297–300 (2010)
22. A. Timoumi, W. Zayoud, A. Sharma, M. Kraini, N. Bouguila, A. Hakamy, N. Revaprasadu, S. Alaya, *J. Mater. Sci: Mater. Electron.* **31**(16), 13636–13645 (2020)
23. A. Timoumi, H. Bouzouita, *Int. J. Renew. Energy Technol. Res.* **2**(7), 188–195 (2013)
24. A. Timoumi, N. Bouguila, J. Koaib, M.K. Al Turkestani, B. Jamoussi, *Mater. Res. Express* **6**(5), 055103 (2019)
25. A. Timoumi, *Graphene* **7**(04), 31 (2018)
26. H. Abassi, N. Bouguila, A. Timoumi, *J. Electron. Mater.* **47**(5), 2519–2525 (2018)
27. A. Timoumi, *IJAREEIE* **2**, 520 (2013)
28. N. Bouguila, A. Timoumi, H. Bouzouita, *Eur. Phys. J. –Appl. Phys.* **65**(2), 20304 (2014)
29. J. Koaib, N. Bouguila, H. Abassi, N. Moutia, M. Kraini, A. Timoumi, C. Vázquez-Vázquez, K. Khirouni, S. Alaya, *RSC Adv.* **10**(16), 9549–9562 (2020)
30. N. Bouguila, A. Timoumi, H. Bouzouita, E. Lacaze, H. Bouchriha, B. Rezig, *Eur. Phys. J. Appl. Phys.* **63**(2), 20301 (2013)
31. T.S. Reddy, M.C.S. Kumar, *Ceram. Int.* **42**(10), 12262–12269 (2016)
32. A. Qasem, S. Alraddadi, E. Al-Amery, H.A. Alrafai, E.R. Shaaban, *Opt. Laser Technol.* **164**, 109488 (2023)
33. P. Monika, Joshi, et al., *Mater. Res. Express* **6**, 086467 (2019)
34. R. Godoy-Rosas et al., *Chalcogenide Lett.* **14**(9), 365–371 (2017)
35. N.A. Kattan, S.A. Rouf, N. Sfina, M. Alanazy, H. Ullah, A. Hakamy, A. Mera, Q. Mahmood, M. A. Amin, *J. Solid State Chem.* **319**, 123820 (2023)
36. S.J. Gnanamuthua, I.K. Punithavathya, S.J. Jeyakumara, P.C. Jobe Prabhakara, K. Parasuramanb, V.S. Nagarethinamc, K. Usharanic, A.R. Baluc, *Acta Phys. Pol. A* **133**, 15–19 (2018)

Publisher’s Note Springer Nature remains neutral with regard to jurisdictional claims in published maps and institutional affiliations.

Springer Nature or its licensor (e.g. a society or other partner) holds exclusive rights to this article under a publishing agreement with the author(s) or other rightsholder(s); author self-archiving of the accepted manuscript version of this article is solely governed by the terms of such publishing agreement and applicable law.